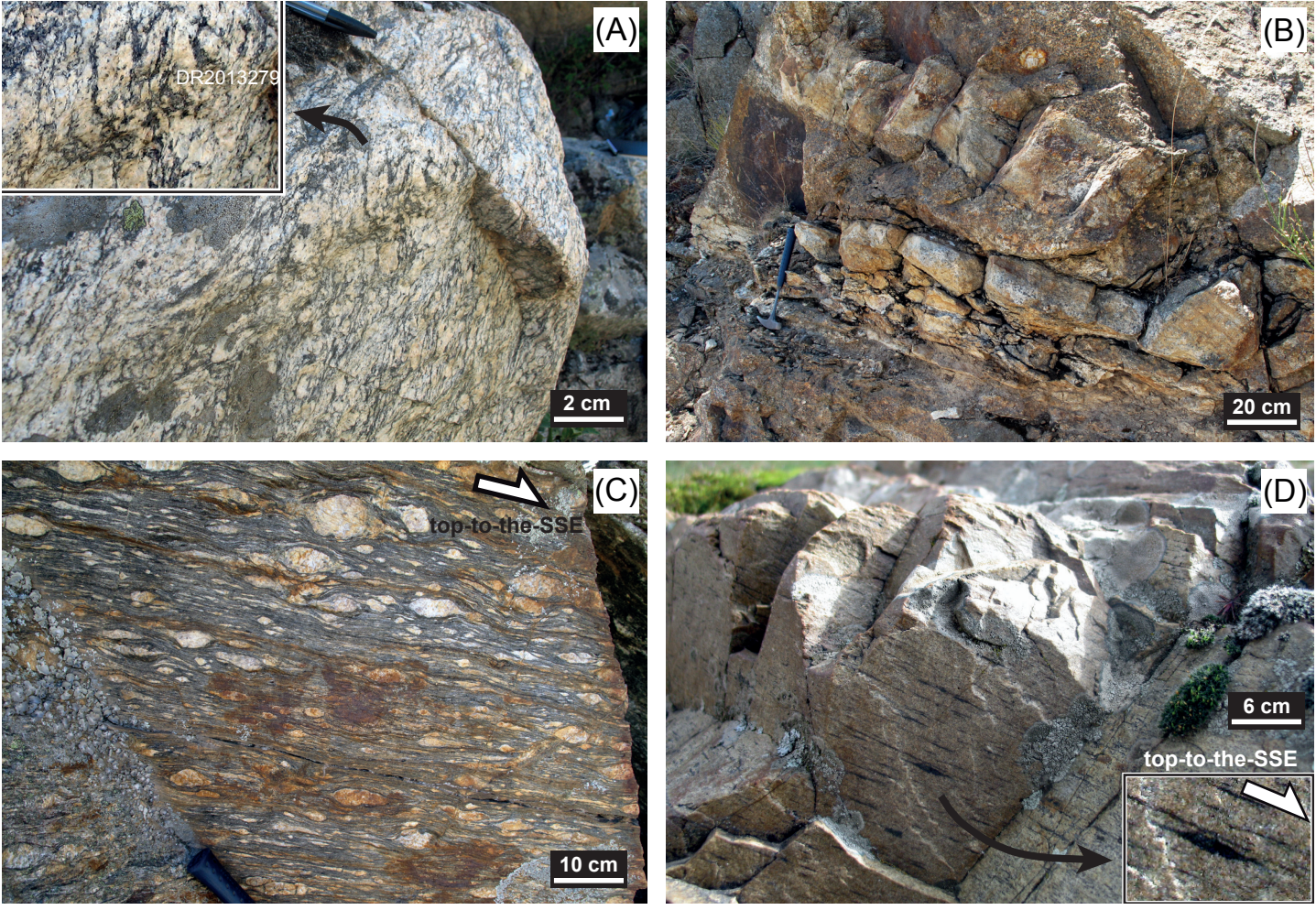

Figure 4 - (A) Granodiorite/adamellite augen orthogneiss showing D_2 crenulation (inset). **(B)** Folded (D_2) aplite/pegmatite dike in the granodiorite orthogneisses. **(C)** Main foliation (S_2) in the monzogranite augen orthogneisses and **(D)** leucogneisses. Note the kinematics indicated by asymmetric feldspar porphyroclasts and melanocratic aggregates (sections parallel to finite stretching lineation).

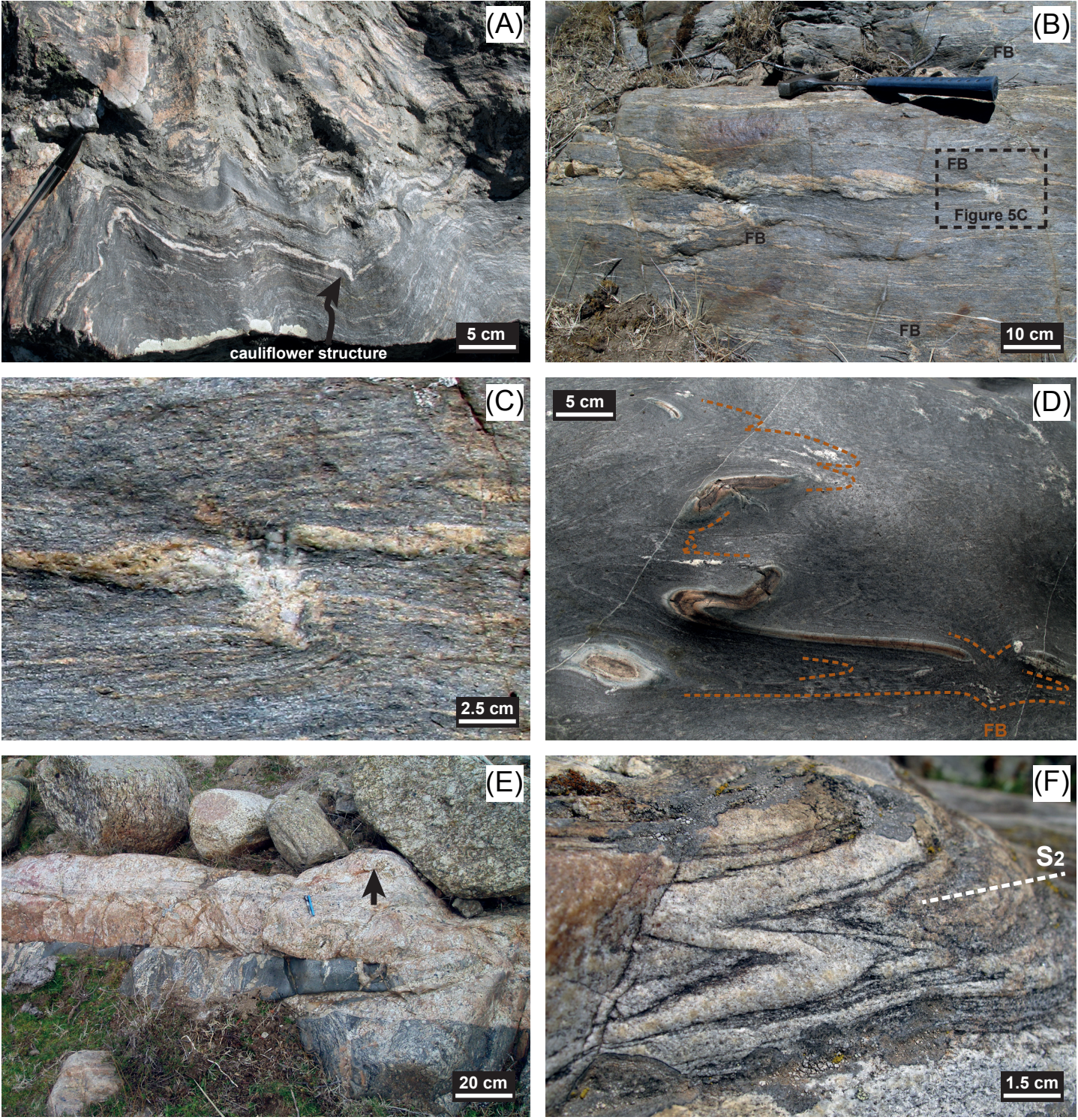

Figure 5- (A) D_3 subvertical crenulation of S_2 in the migmatized paragneisses. Note the development of a crenulation lineation in the upper half part and the way-up criteria (arrow) indicated by cauliflower structures. **(B)** Isoclinally folded (D_2) leucosomes in migmatized paragneisses. Melt-filled boudin necks developed after folding are observed (inset in Figure 5c). **(C)** Inset of a foliation boudinage of S_2 in the migmatized paragneisses (melt-filled neck). See location in Figure 5b. **(D)** Marble lens within migmatized paragneisses. The lens is affected by (1) shearing and boudinage (D_1-D_2), (2) D_2 isoclinal folds, and (3) late-D_2 foliation boudinage. The first boudinage is not coeval with the isoclinal folding, as demonstrated by folded boudin necks (whitish granitic strips between lenses). **(E)** Variscan felsic granitoids and pegmatites cropping out in the core of the Santa María de la Alameda dome. Note the convex up shape of the upper boundary and the flat shape of the lower one. **(F)** D_2 isoclinal folds in paragneisses. FB: Foliation Boudinage

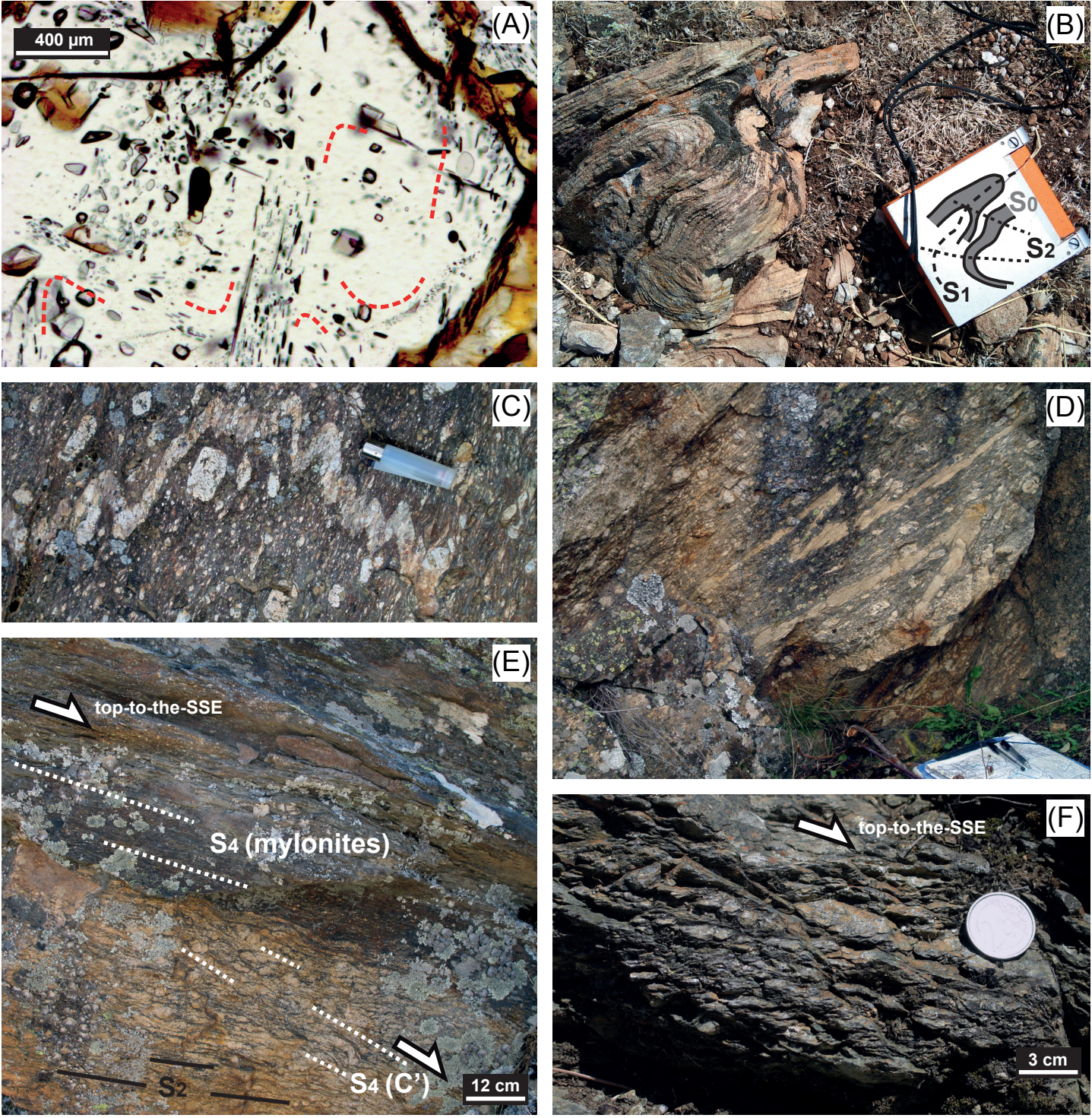

Figure 6 - (A) Mineral fabrics included in a D_2 garnet porphyroblast grown in the paragneisses. The inclusions seem to represent a pre-S_2 crenulation cleavage? **(B)** Marble beds (S_0) depicting the interference between D_2 and previous (D_1), homoaxial folds. See sketch on compass. **(C)** S_2 axial plane foliation formed in a hinge zone of D_2 folds and affecting a pegmatitic dike intruded in monzogranite augen orthogneisses. **(D)** Asymmetrically folded (D_2) fine-grained dikes in the monzogranite augen orthogneisses. The picture shows a normal-to-the fold axes and S_2 view. Note that the micro-fractures of the feldspar porphyroclasts are orthogonal to the foliation and lineation. **(E)** D_4 mylonitic bands (dark colours) bounding a less deformed block of orthogneiss (C´ shear bands) in the Santa María de la Alameda shear zone. **(F)** Inset into the mylonitic bands showing C´-S structures.

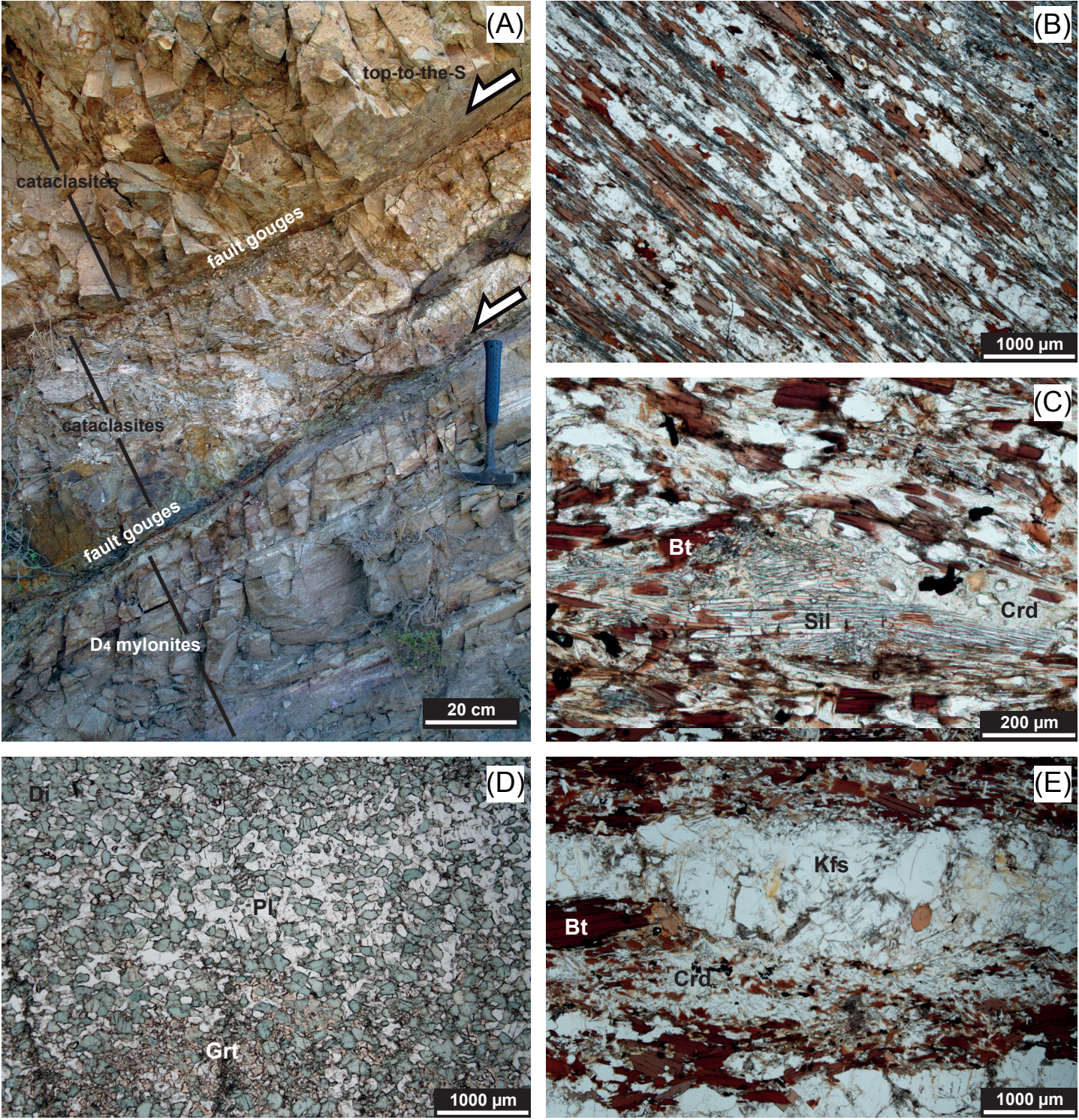

Figure 10- (A) Fault gouges and cataclasites affecting the mylonitic bands in the upper part of the Santa María de la Alameda shear zone. Transition from a ductile to a ductile-brittle regime. **(B)** S_2 tectonic banding in sillimanite + biotite paragneiss. **(C)** Late S_2-cordierite (pinnitised) growing at the expense of S_2-biotite and S_2-sillimanite needles in paragneiss. **(D)** Shape-preferred orientation of mineral grains (S_2) in calc-silicate rocks. Note the porphyroblastic texture of plagioclase. **(E)** Gneissic banding (S_2) in monzogranite augen orthogneiss.

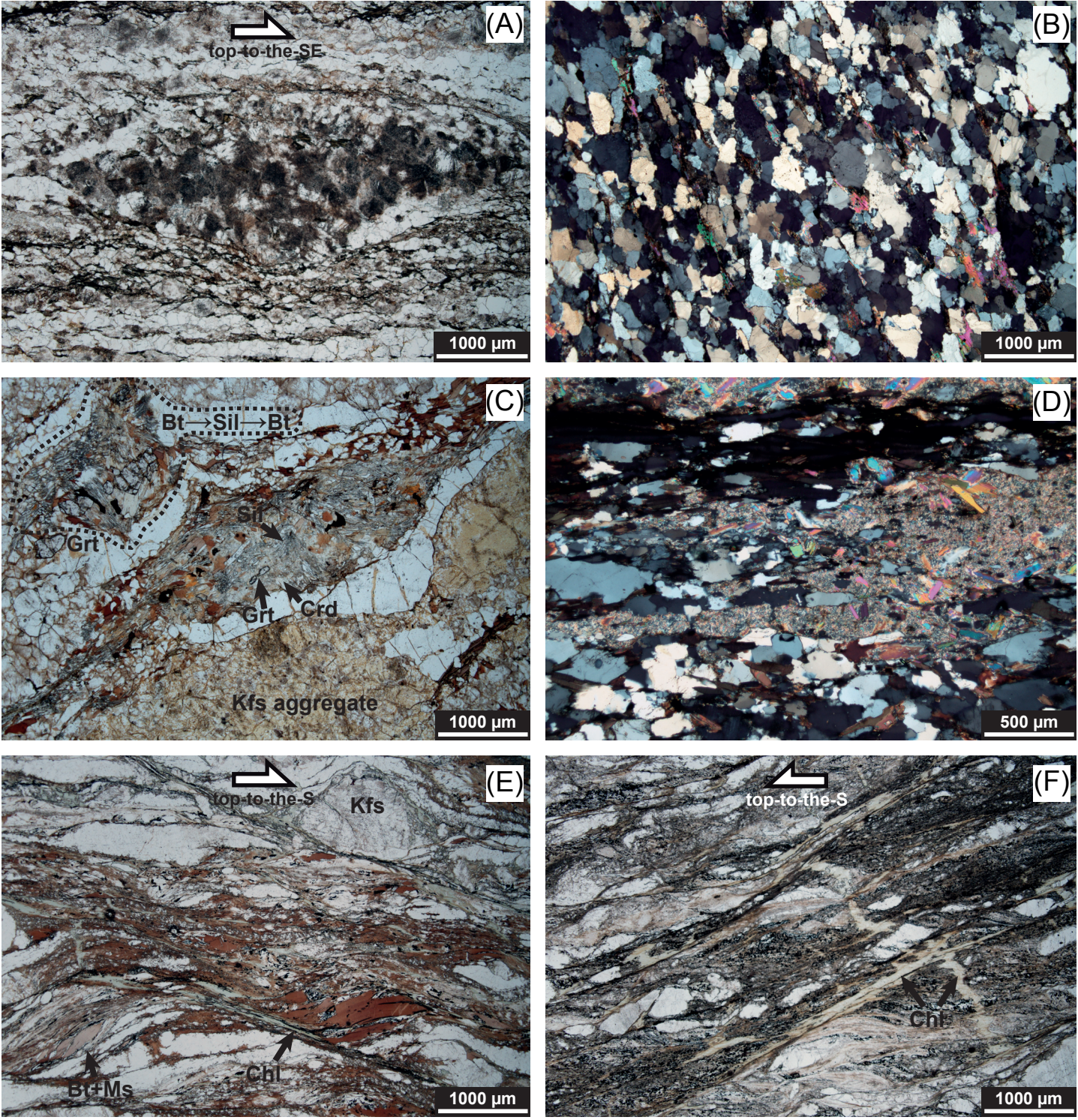

Figure 11- (A) Asymmetric K-feldspar porphyroclast (monzogranitic orthogneiss) transformed into an aggregate of microcline-orthoclase and surrounded by quartz ribbons and layers of aluminosilicate-mica-quartz-feldspar (S_2). **(B)** Main foliation (S_2) in the leucogneisses. **(C)** Transformation of igneous? biotite into S_2-sillimanite (also retrograde to biotite), and growth of late S_2-cordierite at the expense of biotite, garnet, and S_2-sillimanite in monzogranitic orthogneiss. **(D)** Cordierite porphyroblasts, trapping mica and quartz, and parallel to the main foliation (S_2) in monzogranitic orthogneiss. **(E)** Medium-(Bt+Ms) to low-grade (Chl) C'-S mylonites of the Santa María de la Alameda shear zone. Chlorite occurs in C' shear bands. **(F)** Very low-grade (Chl) C'-S mylonites of the Santa María de la Alameda shear zone.